AIAA Journal
Vol. 48, No. 3, March 2010

Dynamic Elastic-Axis Shifting: An Important Enhancement of Piezoelectric Postbuckled Precompressed Actuators

Roelof Vos* and Ron Barrett†
University of Kansas, Lawrence, Kansas 66045

DOI: 10.2514/1.38339

A new actuator arrangement that is designed to protect postbuckled precompressed elements is presented. This actuator arrangement uses through-the-thickness dynamic elastic-axis shifting to protect the convex face of postbuckled precompressed bending actuators at high curvatures, which is important, as postbuckled precompressed elements have been shown to possess simultaneous blocked force and deflection-level increases up to four times those of conventional piezoelectric actuators. This innovation allows this new generation of high-performance piezoelectric actuators to be more robust and less sensitive to tensile failure and depoling on the convex face. As the curvature increases, the elastic axis of the element is shifted dynamically from the center of the laminate through the thickness toward or beyond the convex face of the actuator core, thereby relieving the convex face from tensile loads and effectively stiffening the entire laminate. This dynamic elastic-axis shifting is achieved by adding a facing sheet to the laminate that only carries tensile loads at high curvatures. A silicone spacer between the facing sheet and the actuator element increases the moment of inertia of the facing sheet and increases the effectiveness of the facing sheet. This paper presents an investigation into the effects of the facing-sheet/spacer arrangement on the postbuckled precompressed performance. Analytical models are presented that predict the end rotation at which facing-sheet engagement occurs. Experimental tests were done on a variety of spacer and facing-sheet geometries, demonstrating the dynamic elastic-axis shifting principle for each of the configurations. Deflection testing of dynamic elastic-axis-shifting modified postbuckled precompressed beams was carried out through end rotations in excess of 10° on 10-cm-long piezoelectric benders with good correlation between theory and experiment. It is shown that with a weight penalty of only 12% with respect to the baseline actuator element, the robustness of the postbuckled precompressed beam actuator elements can be significantly increased.

Nomenclature

b	=	actuator width, m
D	=	coupling coefficient, Nm
E	=	electric field, V/m
F_a	=	precompression force, N/m
k	=	constant, N/deg
L	=	length, m
$\tilde{L}$	=	length during deflection, m
m	=	mass, kg
t	=	thickness, m
x	=	principal direction, m
y	=	transverse direction, m
$\tilde{y}$	=	offset from x axis during deflection, m
Δ	=	difference
δ	=	postbuckled precompressed local deflection, deg
κ	=	curvature, deg/m
θ	=	end rotation, deg
σ	=	normal stress, N/m^2

Subscripts

a	=	actuator
fc	=	first contact
fs	=	facing sheet
s	=	substrate
sp	=	spacer
0	=	zero deflection
3	=	through-the-thickness direction

Received 30 April 2008; revision received 18 November 2009; accepted for publication 18 November 2009.

*Currently Assistant Professor, Faculty of Aerospace Engineering, Delft University of Technology, P.O. Box 5058, 2600 GB Delft, The Netherlands. Member AIAA.

†Associate Professor, Department of Aerospace Engineering, 2120 Learned Hall. Senior Member AIAA.

I. Introduction

Adaptive materials have been successfully employed in aviation for more than three decades. Applications ranging from twist active wings to solid-state helicopter rotors, from missile fins to morphing wings, and from guided munition to adaptive hydraulic couplers have all been proven on the bench and in flight on aircraft from the A-10 through the B-2 [1]. The most commonly used adaptive actuators are based on either shape memory materials or piezoelectrics. This first group of materials uses a change in temperature to induce a change in mechanical strain. Even though the active work density of this group of materials is high, their relatively large power-consumption requirements can result in high system weight [2] unless a change in ambient temperature is used as a trigger for actuation [3,4]. Piezoelectric materials have the advantage of having comparatively low power requirements, high bandwidth, and low part count when integrated properly into an aircraft structure [5]. Since conventional piezoelectric actuators trade stroke for applied force, various mechanical arrangements have been employed to increase stroke [6–13]. Although effective, these efforts decreased the total work output and often led to complicated actuator arrangements, lower system-level active work and power density, and an increase in part count.

In recent years, several important advances have been made in a new corner of adaptive materials actuation. These discoveries and inventions are centered on extracting more performance out of existing adaptive materials by simultaneously magnifying both deflection and force capability. One of these approaches centered on increasing the actuator stroke of PZT (lead titanate zirconate) stack actuators by relying on their resonance frequency for amplification [14,15]. By using a buckled-beam motion amplifier, it was shown that angular deflections of a rotor blade flap could be significantly increased without losing control authority [16]. A less complex, less heavy, and less expensive approach is the concept of postbuckled precompression (PBP). Its earliest incarnation was primarily intended to increase the coupling coefficient exhibited by piezoelectric transducer elements [17,18]. Experimental testing showed that (apparent) transfer efficiencies approaching unity could be achieved by axially loading bending elements with forces that approached the buckling load of the beam. In 2002, various actuator configurations were invented that were intended to increase the mechanical work of piezoelectric actuators by using axial loads to increase the coupling coefficient [12]. In 2003, these basic advances were expanded to the realm of aircraft flight control. The first patent application built upon the buckled-beam configuration connected various parts of the beam to flight control effectors on aircraft ranging from subsonic through hypersonic [19]. Since this early filing, the invention has been applied to guided munitions and uninhabited aerial vehicles (UAVs) with a high level of success.

Figure 1 shows three examples of successful applications of PBP elements as flight control actuators. Figure 1a shows the a detail of the PBP-equipped XQ-138 convertible UAV. Figure 1b presents the application of PBP actuators in a morphing wing configuration to enable roll control on a subscale UAV. Figure 1c demonstrates the application of a PBP element in a control surface of a micro aerial vehicle. Other applications of PBP actuators include PBP-actuated synthetic jet actuators and a novel wing twisting device [20,21]. Analytical, semi-analytical, and finite element modeling were shown to accurately capture the behavior of PBP elements [22,23].

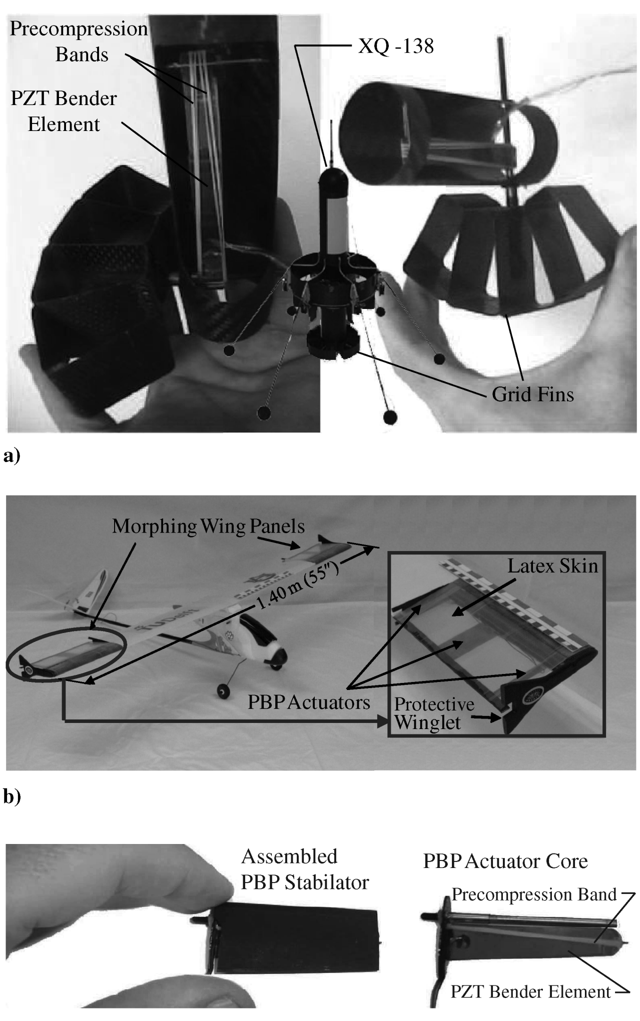

Fig. 1 Application of PBP flight control actuators: a) PBP actuator element in grid fin test-rig assembly for application on XQ-138 [24], b) subscale UAV employing PBP-actuated morphing panels [25], and c) PBP-actuated flight control surface for micro aerial vehicle [26].

The concept of postbuckled precompression is relatively straightforward in that a slender beam is loaded axially to enhance bending deflections as the axial load and imperfection levels are increased. Because the imperfection level can be controlled by varying the active commanded moments generated by the adaptive elements placed on or in the beam, extremely large deflections can be commanded. In other words, the axial force creates a low net passive stiffness (LNPS) or zero net passive stiffness (ZNPS) in the beam. Figure 2 shows the basic PBP actuator principle and the effect of axial compression on the amount of deflection. A typical bender element configuration shows the usual centrally located substrate with a pair of piezoelectric elements bonded to either side so that bending deformations can be introduced. If one considers the shape of Fig. 2, it can be seen that the tensile stresses on the upper face of the upper piezoelectric element can induce element depoling and/or fracture at high deformation levels.

The reader is asked to consider three alternative PZT bender elements, each designed for the same amount of work output, but at various combinations of maximum applied moment and end rotation. Their design spaces can be shown in the applied-moment end-rotation diagram of Fig. 3. Within each design space of these actuator elements, a combination of the maximum *rated* applied moment and end rotation can be achieved. However, the actual maximum applied moment decreases linearly with end rotation, forming the absolute limits of each of the bender elements. Superposition of each of these limiting lines results in an absolute boundary of the design space within which all PZT bender elements of that particular work output operate. By creating a ZNPS PBP actuator, there is essentially no energy required to deform the structure, and the maximum applied moment can be generated throughout the range of end rotations, until the element fractures. In practice, the LNPS PBP actuator uses part of this energy to strain the structure. However, significant higher applied moments can be applied at increased end rotations. This can result in a significant expansion of the design space of the original actuator, as shown in Fig. 3.

As curvatures are increased to achieve high end rotations, the tensile stresses in the convex face form the end-rotation boundaries as depoling and tensile failure considerations come into play. One useful mechanism that has been shown to work quite well to expand these PBP boundaries is the use of coefficient of thermal expansion (CTE) mismatch between substrate and actuator elements. The residual stresses that exist as a result of a high-temperature cure of the laminate ensure that the PZT elements are in precompression. Although quite effective in expanding the end-rotation envelope, there are still difficulties at high curvature levels with simply using CTE mismatch for precompression of PBP elements. Accordingly, a new approach is needed to prevent tensile stresses from being experienced on the convex actuator face.

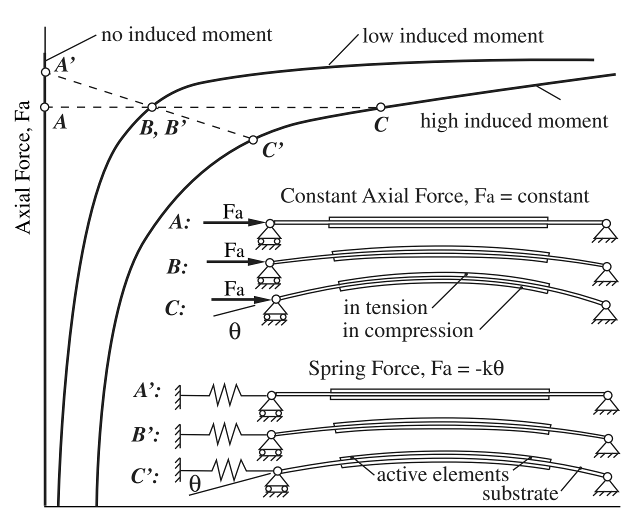

Fig. 2 Operating principle of a PBP actuator element.

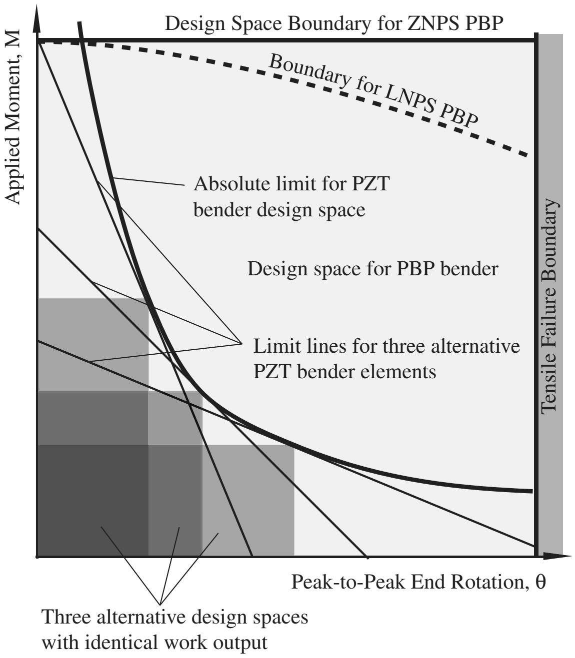

Fig. 3 Expansion of moment-deflection boundaries made possible by PBP actuator configurations.

This new approach is the subject of this article and relies on the dynamic elastic-axis shifting (DEAS) of the actuator element. The DEAS method has a profound effect on the behavior of the PBP element, as it stiffens the element at high curvatures by shifting the elastic axis from the center of the bender element toward or beyond the convex actuator face [19]. This principle is achieved by adding a facing sheet to the convex face of the actuator that only carries tensile load at high curvatures, thereby relieving the ceramic PZT sheet (see Fig. 4). By adding a highly compliant, low-stiffness spacer between the substrate and the facing sheet, the effect of facing-sheet engagement on the stiffness of the laminate can be tailored. In the present incarnation, the spacer is connected to the bender element at its center. The facing sheet is offset from the spacer and air resides between them. If the DEAS system is designed properly such that the facing-sheets engage before the tensile face of the element fails, it shifts the elastic axis so far that the convex actuator face only sees extremely small tensile stresses while the concave face experiences compressive stresses orders of magnitude greater.

DEAS is an important improvement of PBP actuators because it introduces a sudden increase in bending stiffness as the curvature increases. When the loading on the actuator is constant, the stiffening resists further curving. Additional measures such as external bump stops (as were used in all applications of Fig. 1) can be omitted, resulting in an additional weight savings and complexity reduction. The addition of a facing-sheet arrangement to the PBP element increases the overall robustness of the actuator, making it even more competitive than conventional state-of-the-art flight control actuators.

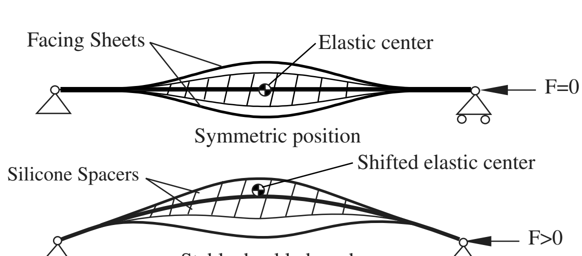

Fig. 4 Sketch of dynamic elastic-axis shifting in PBP actuator because of facing-sheet application (side view).

II. Facing-Sheet Engagement Modeling

To design PBP actuator elements with DEAS, it is important to be able to predict at which curvatures (or end rotations) facing-sheet engagement occurs. It is evident that this is dependent on the geometry of both the spacer and the facing sheet. In Fig. 5 the process of facing-sheet engagement is presented in five subsequent sketches. Initial beam imperfections are introduced by applying an electric field over the PZT elements. The addition of an axial force increases end rotations until first contact (fc) is reached. Beyond θ_{fc} the beam, spacer, and facing sheet behave as one laminate. Based on the principle laid out in Fig. 5, the following subsections present two simple mathematical models that correlate the facing-sheet/spacer geometry to the end rotation of first contact.

A. Facing Sheet

Considering a cosine form factor for the facing sheet, which has been experimentally shown to be accurate to within 3% of the actual form factor, the following expression describes the shape of the facing sheet at zero PBP beam deflection as a function of horizontal coordinate, x, the length of the spacer at zero deflection, $L_{0\mathrm{sp}}$, and the maximum height of the facing sheet, $y_{0\mathrm{fs}}$:

$$y_{\mathrm{fs}}(x) = \frac{y_{0\mathrm{fs}}}{2}\left[1 - \cos\left(\frac{2\pi x}{L_{0\mathrm{sp}}}\right)\right] \tag{1}$$

From experiments performed and reported in Sec. IV, it was determined that the shapes of the actual facing sheets used experimentally possessed vertical displacements that differed in length by no more than 3% of from the cosine form factor described in Eq. (1). See Fig. 5 for a schematic representation of facing-sheet/spacer arrangement, facing-sheet engagement, and nomenclature.

B. Substrate

If one assumes a parabolic form factor for the substrate, which is also a very close approximation to the actual measured shapes of the substrate centerline, then the following relationship is seen between the centerline of the substrate, the horizontal coordinate x, and the end tab rotation angle θ:

$$\tilde{y}_s(x) = \left(x - \frac{x^2}{L_{\mathrm{sp}}}\right)\tan\theta \tag{2}$$

C. Spacer

Considering that the spacer is attached to neither the substrate nor the facing sheet, it fundamentally holds its thickness dimensional characteristics through deflection to first contact. Accordingly, using Eq. (2), the height of the upper face of the spacer during deflection, $\tilde{y}_{\mathrm{sp}}(x)$, can be approximated by the following expression:

$$\tilde{y}_{\mathrm{sp}}(x) = y_{\mathrm{sp}}(x) + \tilde{y}_s(x) = \frac{y_{0\mathrm{sp}}}{2}\left[1 - \cos\left(\frac{2\pi x}{L_{\mathrm{sp}}}\right)\right] + \left(x - \frac{x^2}{L_{\mathrm{sp}}}\right)\tan\theta \tag{3}$$

From Eq. (3), it can be seen that the height of the upper face of the spacer during deflection is approximated by the height of the spacer with zero deflection, y_{sp}, and the shape of the substrate centerline during deflection, $\tilde{y}_{\mathrm{sp}}$.

D. First-Order First-Contact Estimation by Center-Point Matching

If one assumes that at small deflections, the actual mode shapes of the facing sheet, beam, and spacer possess manufacturing irregularities near the edges, making the shapes of the three very similar, then one can assume that contact occurs when the upper surface of the spacer first reaches the y coordinate of the facing sheet at the midpoint of the PBP beam, such that

$$\tilde{y}_{\mathrm{fs}}|_{x=L_{\mathrm{sp}}/2} = \tilde{y}_{\mathrm{sp}}|_{x=L_{\mathrm{sp}}/2} \tag{4}$$

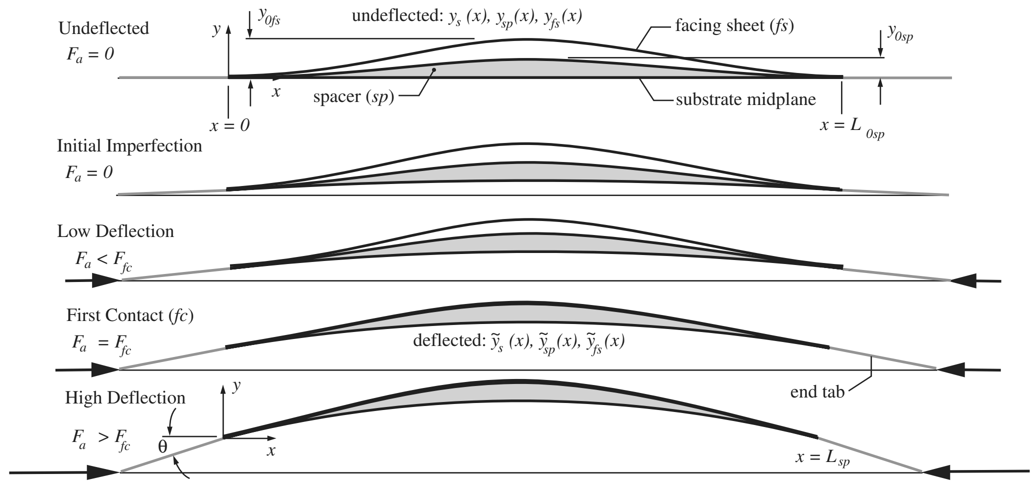

Fig. 5 Schematic representation of facing-sheet engagement and definitions.

Unlike the imperfection levels mentioned in Sec. I, which are controlled deviations from a perfectly straight beam by inducing a uniform bending moment, manufacturing irregularities are typically one to three orders of magnitude smaller than commanded imperfections. Accordingly, these manufacturing irregularities, although artifacts of real test articles, do not make significant contributions to the overall deformed shapes of the commanded structural deformations. Substituting Eqs. (1) and (3) and keeping in mind that $L_{0\text{sp}} \to L_{\text{sp}}$ in buckled mode yields a first-order approximation for contact,

$$\tan\theta_{\text{fc}} = \frac{4}{L_{\text{sp}}}(y_{0\text{fs}} - y_{0\text{sp}}) \tag{5}$$

From Eq. (5) it can be seen that by this first-order estimation, the tab angle θ is just a simple function of the air gap between the upper surface of the spacer and the facing sheet, divided by the length of the spacer.

E. Second-Order First-Contact Estimation by Length Matching

A more accurate method of determining the onset of first contact can be obtained by matching the lengths of the facing sheet and the upper surface of the spacer. The length of the facing sheet can be obtained by integrating Eq. (1) as follows:

$$L_{\text{fs}} = \int_0^{L_{\text{sp}}} \sqrt{1 + \left(\frac{\mathrm{d}y_{\text{fs}}(x)}{\mathrm{d}x}\right)^2}\,\mathrm{d}x = \int_0^{L_{\text{sp}}} \sqrt{1 + \left[\frac{y_{0\text{fs}}\pi}{L_{\text{sp}}}\sin\left(\frac{2\pi x}{L_{\text{sp}}}\right)\right]^2}\,\mathrm{d}x \tag{6}$$

If one integrates Eq. (1) and assumes that $y_{0\text{fs}} \ll L_{\text{sp}}$, then the following approximation of facing-sheet length can be obtained:

$$L_{\text{fs}} = \tilde{L}_{\text{fs}} \simeq L_{\text{sp}}\left[1 + \left(\frac{y_{0\text{fs}}}{2L_{\text{sp}}}\right)^2\right] \tag{7}$$

The above approximation has been shown to be good to within 1%, given facing-sheet offset levels $y_{0\text{fs}}$ of no more than 10% of the spacer length, L_{sp}. From experiments performed and reported in Sec. IV, it was determined that the length of the actual experimental facing sheets, L_{fs}, were indeed within 1% of the estimated facing-sheet length given the above restriction on $y_{0\text{fs}}$.

Given the comparatively complicated mode shape of the upper surface of the spacer, an elegant simplification as shown above in Eq. (6) is not possible. Still, one can solve exactly for the length by integrating the mode shape:

$$L_{\text{fs}} = \int_0^{L_{\text{sp}}} \sqrt{1 + \left(\frac{\mathrm{d}y_{\text{sp}}(x)}{\mathrm{d}x}\right)^2}\,\mathrm{d}x = \int_0^{L_{\text{sp}}} \sqrt{1 + \left[\frac{y_{0\text{sp}}\pi}{L_{\text{sp}}}\sin\left(\frac{2\pi x}{L_{\text{sp}}}\right) + \left(1 - \frac{2x}{L_{\text{sp}}}\right)\tan\theta\right]^2}\,\mathrm{d}x \tag{8}$$

Because it can be shown that the lengths of the facing sheet and upper surface of the spacer for equal midpoint thicknesses are within 0.04% for end rotations up through even 10°, the lengths of the upper surface of the spacer can be equated to the facing-sheet length as follows:

$$\tilde{L}_{\text{fs}} = L_{\text{fs}} = L_{\text{sp}}\left[1 + \left(\frac{y_{0\text{fs}}}{2L_{\text{sp}}}\right)^2\right] \simeq \tilde{L}_{\text{sp}} = L_{\text{sp}}\left[1 + \left(\frac{y_{0\text{fs}}}{2L_{\text{sp}}}\right)^2\right] = L_{\text{sp}}\left[1 + \left(\frac{y_{\text{sp}} + \frac{L_{\text{sp}}}{4}\tan\theta}{2L_{\text{sp}}}\right)^2\right] \tag{9}$$

Of course, it makes sense that the above estimation degenerates to Eq. (5) upon solution. However, for a higher level of accuracy, Eqs. (6) and (8) can be equated. As noted previously, whether using Eqs. (6) and (8) or Eq. (5), for the deflections considered in this paper and given current manufacturing capabilities, the solution methods bear the similar levels of relevance against experimental data.

III. Prototype Description

The PBP actuator element under consideration was based on the conventional bimorph PZT actuator laminate, as displayed in Fig. 6. It consisted of two 192 μm PZT-5A sheets bonded to either side of a 76 μm aluminum substrate. The bonding layer between PZT and the aluminum consisted of Hysol 9420, and E-glass reinforced epoxy end tabs were added to either side of the substrate next to the PZT sheets to provide structural area to bond the facing sheets to. To ensure a smooth outer actuator surface (which was important for the functionality of the DEAS concept), 25-μm-thick steel leads were attached to the

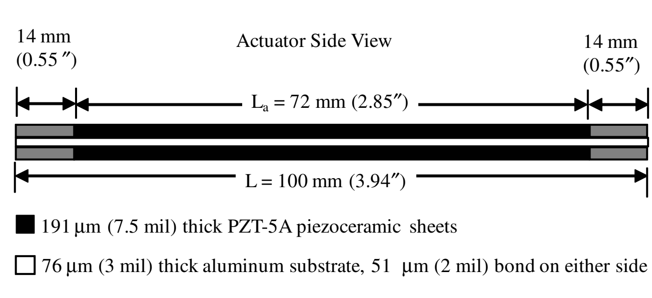

Fig. 6 Typical PBP bender configuration.

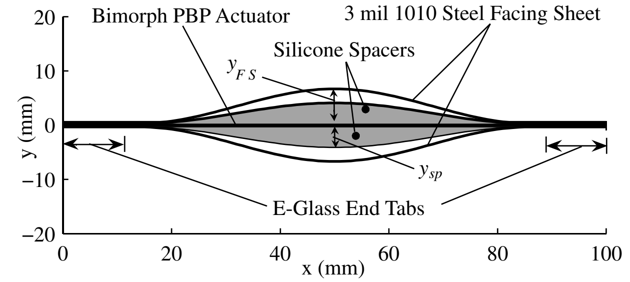

Fig. 7 Bimorph PBP actuator with facing sheets; dimensions and definitions (side view).

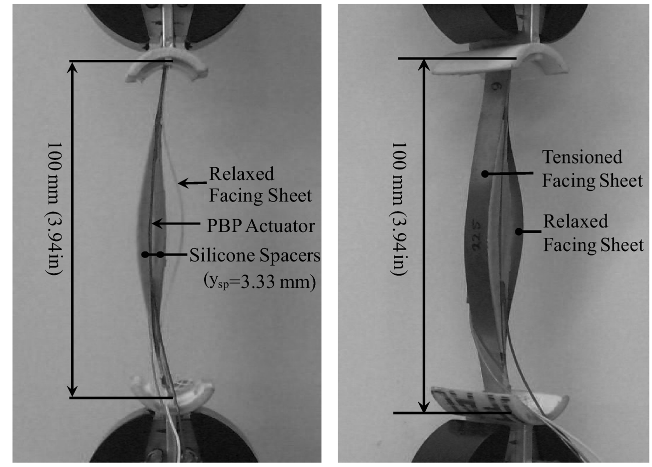

Fig. 8 Experimental setup.

electrode faces of the actuator. The electrodes were electrically insulated by adding a 51 μm polyester tape layer on top of them.

Dynamic elastic-axis shifting in PBP actuators was achieved by adding 76 μm facing sheets to either side of the actuator. In the initial state, both facing sheets formed a cosine shape with a maximum offset y_{fs} from the actuator surface (see Fig. 7). Between the actuator face and the facing sheet, a highly compliant silicone spacer was positioned that also exhibited a cosine shape with a peak displacement from the actuator surface, y_{sp}. The low stiffness (180 kPa) of the silicone spacer provided a negligible effect on the amount of bending stiffness of the beam. When the element bent due to a compressive force applied in axial direction (as in Fig. 2), the facing sheet at the convex face made contact with the silicone spacer, which loaded the facing sheet in tension and the actuator element in compression, relieving the tension-sensitive convex PZT sheet. In this process, the elastic axis shifted through the thickness of the laminate toward or beyond (depending on y_{sp}) the convex face of the actuator (see Fig. 4).

IV. Experimental Testing and Results

To map out the influence of the facing-sheet geometry on the behavior of the PBP actuator, a series of tests were conducted. The experimental setup consisted of a PBP element in vertical pin–pin configuration in an axial compression tool. By moving the top end of the actuator downward, the compression tool applied axial force to the actuator and forced it to bend. Simultaneously, both axial force and vertical displacement were recorded (with an accuracy of 0.1 μm and 0.1 mN, respectively). Vertical displacement Δx was then correlated to end rotation θ with the assumption that the mode shape of the PBP element resembled an arc. This relationship was determined empirically using laser reflection techniques and yielded $\Delta x = 0.006\theta(\theta + 4.6)$, where θ was measured in degrees (accuracy of 0.1°), and Δx was in millimeters. Since charged PZT actuators are sensitive to creep, the compression test on the PBP actuator elements was carried out rapidly: within 3 s after the voltage was applied, all data was taken. Figure 8 shows the general layout of the test.

To investigate the influence of spacer height y_{sp} and facing-sheet offset y_{fs} on the force-deflection diagram, various test specimens were prepared and tested. Six PBP bender elements were constructed with various facing-sheet offsets. In addition, five different spacers were fabricated of different heights. Not all combinations of facing sheet and spacer could be tested, because either they were geometrically incompatible (i.e., the spacer was too big to fit under the facing sheet) or the end rotation at which engagement occurred was beyond the end rotation at which tensile failure of the element occurred. In total, 13 different combinations were tested at four individual field strengths E_3 (130, 260, 390, and 520 V/mm). The objective of the test was to investigate the influence of the facing sheets and to see whether the predictions of first contact (Sec. II) correlated to what was seen in the experiment.

The results of the test, together with the first- and second-order predictions of facing-sheet engagement, are shown in Table 1 and are discussed later in this section. In Fig. 9, the results of three experiments at an electric field of $E_3 = 130$ V/mm are demonstrated. The solid curve demonstrates the exponential increase in end rotation that is obtained when an axial force is applied to the element. On this line, the circular and square markings demonstrate the predicted end rotations at which first contact would occur according to the first-order [Eq. (5)] and second-order [Eqs. (6) and (8)] models, respectively. The dashed lines are the experimental results from the PBP/DEAS test, where the facing sheet and spacers were in place. Three different values of $\Delta y = y_{\mathrm{fs}} - y_{\mathrm{sp}}$ are displayed in this plot, clearly showing that the larger the air gap between the spacer and the facing sheet, the larger the end-rotation angle at which engagement occurred. It can also be observed that the onset was quite smooth at lower values of Δy, whereas at values closer to the fraction boundary, the onset was more abrupt and the force-rotation curve displayed more of a kink when the facing sheet engaged.

The functionality of the facing sheets is obvious from this figure, in that after engagement, the stiffness of the actuator element is increased significantly such that it stays clear of the fracture boundary, even at increased compressive force. Regardless of spacer/facing-sheet geometry, the stiffening of the element was very pronounced in all of the experiments upon facing-sheet engagement ($\theta > \theta_{\mathrm{fc}}$). A clear increase in axial force was observed as the facing sheet touched the spacer and started to carry part of the load. In general, the point of first contact shifted backward when the initial distance between the spacer and facing sheet was increased. Prediction of first contact is fairly good in the case of $\Delta y/L = 1.12$ and 2.92% but shows a significant discrepancy for $\Delta y/L = 1.80\%$.

By examining the data of Fig. 9, a method of determining contact angle θ_{fc} could be divined. This method was termed the median slope technique (MST) and was based on the slope halfway between the two principal slopes on the knee of the rise during transition from free PBP to constrained PBP. The contact angle was defined at the point at which this median slope occurred. In Sec. II, two models were presented to predict the angle of first contact. Considering a working length of $L_{\mathrm{sp}} = 72$ mm, a comparison of predicted contact angle as a function of offset distance $y_{\mathrm{fs}} - y_{\mathrm{sp}}$ was obtained via Eq. (5). Equations (6) and (8) predicted the angle of first contact by correlating the lengths of the facing sheets and the lengths of the upper face of the spacer. By using the MST to determine the end rotation at which first contact occurred, a comparison was made between the experimental data and the predictions of Eq. (5) and Eqs. (6) and (8). Table 1 gives an overview of the DEAS onset and its relation to $\Delta y/L$, as well as the comparison with the first- and second-order models.

The experimental and theoretical values of the DEAS onset angle are graphically represented in Fig. 10. As can be seen from this figure, the experimental data showed substantial scatter. Possible causes for this scatter included manufacturing imperfections and the nonuniform engagement of the facing sheet, which resulted in an incorrect determination of the engagement end rotation. A linear regression of the data resulted in a product-moment correlation coefficient of 0.805. As a whole, the agreement was fairly good, with the slope of the least-squares linear fit matching the slope of the predicted angle of first contact almost exactly, with a 0.3° offset. Curiously enough,

Table 1 Results of DEAS experiments

y_{fs}/L, %	y_{sp}/L, %	$\Delta y/L$, %	θ_{fc}, exp.	θ_{fc}, Eq. (5)	θ_{fc}, Eqs. (6) and (8)	$\Delta m/m_a$, %
4.19	1.27	2.92	10.1°	9.2°	9.4°	127
4.19	1.65	2.54	6.9°	8.0°	8.4°	139
4.19	2.77	1.42	3.4°	4.5°	5.0°	177
4.57	1.65	2.92	9.4°	9.2°	9.5°	139
4.57	2.77	1.80	5.4°	5.7°	6.3°	177
4.57	3.45	1.12	4.0°	3.6°	4.1°	200
5.46	2.77	2.69	8.3°	8.5°	9.1°	177
5.46	3.45	2.01	6.1°	6.4°	7.0°	200
5.46	4.06	1.40	3.5°	4.4°	5.1°	221
6.35	3.45	2.90	7.2°	9.1°	9.9°	200
6.35	4.06	2.29	5.0°	7.2°	8.0°	221
6.60	4.39	2.21	5.0°	7.0°	7.8°	232

the higher-fidelity model considering Eqs. (6) and (8) provided poorer correlation with experiment.

Considering Eqs. (6) and (8) as the triggering condition for engagement of the facing sheet, at the center of the beam, the elastic-axis shift with end rotation can be seen in Fig. 11. From Fig. 11, it is clear that the elastic axis dynamically shifted from the center of the PBP beam to a distance more than two beam thicknesses above the convex face of the PBP beam at the longitudinal center of the actuator element.

In Table 1, the mass that was added to the actuator by the facing-sheet/spacer arrangement is scored in the column under $\Delta m/m_a$. For an actuator element employing two spacers, the relation between y_{sp}/L and Δm_{sp} is as follows:

$$\Delta m_{sp} = 2\rho_{sp} b_{sp} \int_0^{L_a} \frac{y_{sp}}{2}\left[1-\cos\left(\frac{2\pi x}{L_a}\right)\right] \mathrm{d}x = \rho_{sp} b_{sp} y_{sp} L_a \quad (10)$$

The increase in weight caused by the facing sheet itself was identical for all arrangements and amounted to 1.26 g. Since weight is one of the primary optimization parameters in flight control actuator design, an effort was made to reduce it without losing the benefits of the DEAS on the robustness of the actuator.

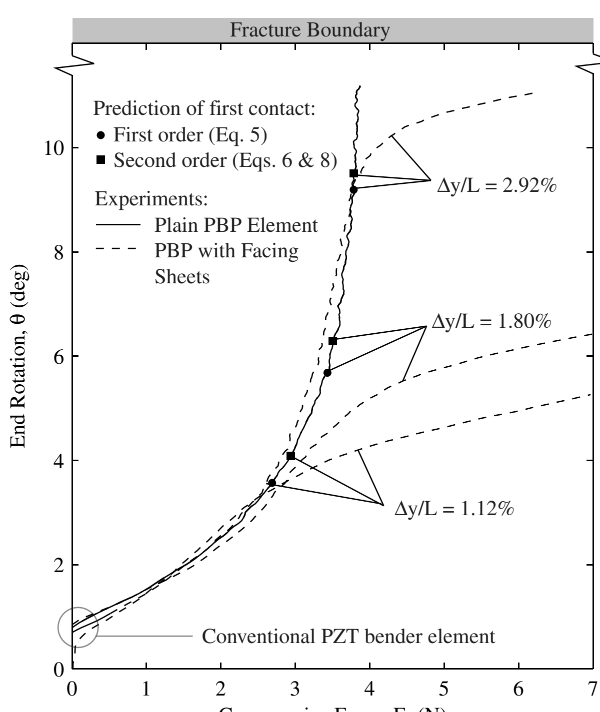

Fig. 9 Example of experimental results for PBP element with $y_{fs}/L = 4.6\%$, $E_3 = 130$ V/mm, $L = 100$ mm, and $b = 10$ mm.

V. Minimizing Weight of PBP/DEAS Actuator

From Table 1, it is clear that the thinnest spacer gave the least weight increase, and its behavior was still comparable with thicker spacers. In an attempt to reduce the total weight of the actuator even further, the 76 μm steel facing sheet was replaced by a 25.4 μm steel facing sheet and a 74 μm unidirectional carbon-epoxy facing sheet, respectively. This reduced the weight of the facing sheets by 66 and 72%, respectively, and did not have a particular effect on the results. To reduce weight even further, the widths of both the facing sheet and the spacer were reduced to 20% of the actuator width, using a 69-μm-thick carbon-epoxy facing sheet. Results are shown in Fig. 12 for a 1.75 mm spacer. The result of this experiment shows that DEAS was still very pronounced and started at $\theta_{fc} = 8.7°$.

Two interesting observations can be made from Fig. 12. First, the slope of the curves when θ_{fs} is surpassed is less steep for this configuration than for the configurations for which the results are displayed in Fig. 9. The smaller slope was caused by the decreased contact area between spacer and facing sheet, which was reduced by 80% with respect to the original arrangement. The smaller contact area gave the spacer a lower resistance to the compressive force induced by the facing sheet (i.e., lower effective compressive stiffness), resulting in a less pronounced DEAS effect.

Second, the curve displays a kink at θ_{fs}, rather than a gentle change in slope as for the previous configurations. The kink in the curve indicates that the facing sheet almost simultaneously touched the spacer everywhere on its surface. Because of small misalignments between spacer and facing sheet caused by manufacturing flaws, this

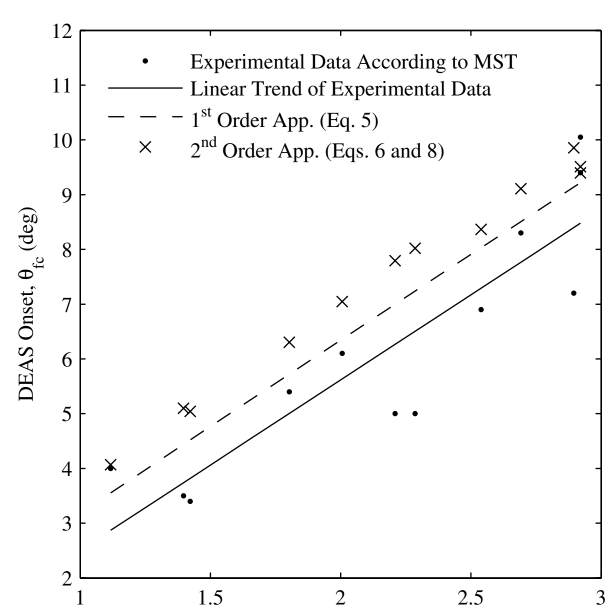

Fig. 10 Empirical relationships between DEAS onset and facing-sheet offset.

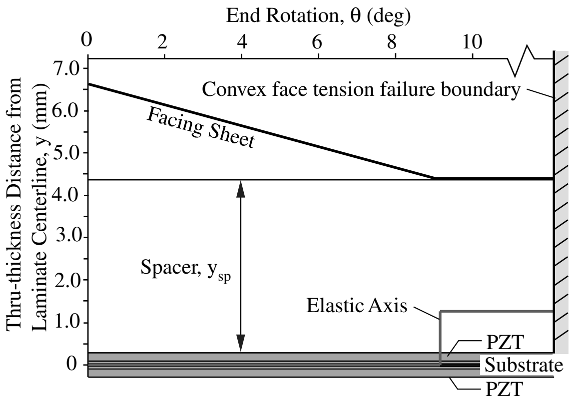

Fig. 11 Predicted dynamic elastic-axis shift at longitudinal centerline of actuator element: $y_{fs} = 6.6$ mm and $y_{sp} = 4.4$ mm.

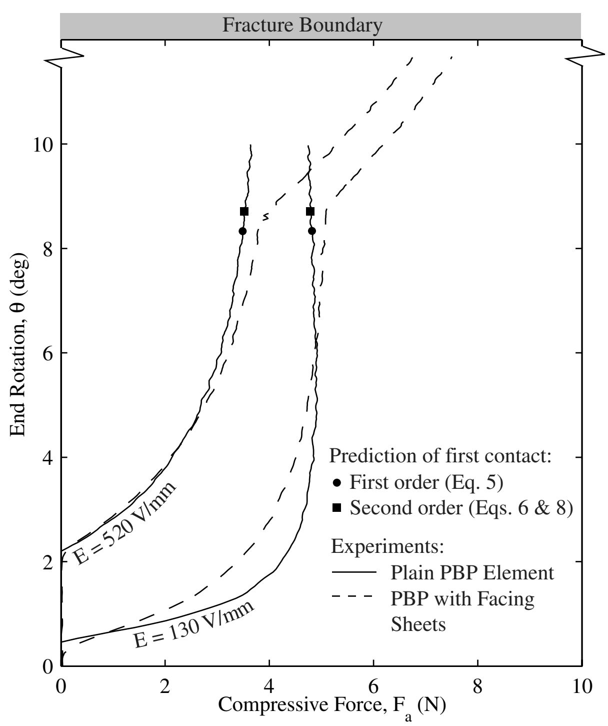

Fig. 12 Results for minimum weight facing-sheet arrangement.

uniform onset could not be achieved in the wider-facing-sheet arrangements of Fig. 9. This resulted in a more gentle onset of the wider-facing-sheet configurations, which is generally not desirable, as it is less predictable. From Fig. 9, it can be seen that the second-order first-contact estimation accurately (less than 0.1%) predicted the end rotation at which the facing-sheet onset occurred. The first-order theory predicted within 5% of the measured angle of facing-sheet onset. The total mass increment due to spacer and facing sheet in this configuration amounted to 0.39 g, which was only a 12% increase with respect to the baseline PBP actuator.

VI. Conclusions

PBP actuator elements have shown superior behavior over conventional piezoelectric bender elements. By applying an axial force, both end-moment and end-rotation levels were magnified simultaneously up to a factor of 4, resulting in highly curved actuator elements. To prevent the convex actuator face from mechanical fracture and depoling, a new concept that relied on through-the-thickness shifting of the elastic axis was conceived. This concept composed of adding a set of facing sheets on either side of the element that would only carry tensile loads at high curvatures and thereby relieve the tension-sensitive convex actuator face. Facing-sheet engagement effectively stiffened the actuator, making it less prone to bending. By adding low-stiffness silicone spacers between the facing sheet and the actuator element, the amount of stiffening upon facing-sheet engagement could be adjusted. Experimental tests were done on a variety of spacer and facing-sheets geometry, demonstrating the DEAS principle for each of the configurations. It was shown that the first-order theory gave a better prediction than the higher-fidelity model of facing-sheet engagement. Analytic modeling of the PBP element with DEAS showed the same trends as were seen in the experiments. Although the experimental data showed considerable scatter due to the nonlinear nature of the problem, several DEAS onset angles were predicted to within 2%. However, higher-fidelity models are required to properly capture the behavior of the elements during axial loading. Experimental testing showed that DEAS onsets could be designed to occur at deflections as little as 2 deg to more than 8 deg of end rotation. Similarly, DEAS stiffnesses following onset were demonstrated to be as much as an order of magnitude greater than simple PBP beam stiffnesses, with a shift of elastic axis completely off the PBP beam itself at high deflections. In an effort to save weight on spacer/facing-sheet arrangement, the widths of both spacer and facing sheet were reduced to 20% of the actuator width, and a 69 μm carbon-epoxy facing sheet was used. Because of the smaller spacer width, uniform onset of the facing sheet was ensured, which was shown to correlate accurately to the higher-fidelity model predicting the end rotation of facing-sheet engagement. This configuration added only 12% to the total actuator weight. The minor increase in weight and the increased actuator robustness make the facing-sheet-equipped PBP actuator an excellent replacement for flight control actuators in subscale UAVs.

Acknowledgments

The research presented in this paper was sponsored by the Aerospace Engineering Department of the University of Kansas. The authors would like to acknowledge the great contribution of Paolo Tiso to the work that is presented in this paper.

References

[1] Barrett, R., "Adaptive Aerostructures—The First Decade of Flight on Uninhabited Aerospace Systems," *Proceedings of SPIE: The International Society for Optical Engineering*, Vol. 5388, Sept. 2004, pp. 190–201.
doi:10.1117/12.536681 pp.190-201

[2] Barrett, R., Burger, C., and Melian, J., "Recent Advances in Uninhabited Aerial Vehicle (UAV) Flight Control with Adaptive Aerostructures," *Proceedings of the 2001 Conference on Smart Technology Demonstrators and Devices*, Inst. of Physics, Philadelphia, June 2002, pp. 1–11.

[3] Mabe, J. H., Calkins, F. T., and Butler, G. W., "Boeings Variable Geometry Chevron, Morphing Aerostructure for Jet Noise Reduction," 47th AIAA/ASME/ASCE/AHS/ASC Structures, Structural Dynamics, and Materials Conference, AIAA Paper 2006-2142, Newport, RI, 1–4 May 2006.

[4] Turner, T. L., Buehrle, R. D., Cano, R. J., and Fleming, G. A., "Modeling, Fabrication, and Testing of a SMA Hybrid Composite Jet Engine Chevron Concept," *Journal of Intelligent Material Systems and Structures*, Vol. 17, No. 6, June 2006, pp. 483–497.
doi:10.1177/1045389X06058795

[5] Vos, R., Barrett, R., DeBreuker, R., and Tiso, P., "Post-Buckled Precompressed (PBP) Elements: A New Class of Control Actuators for Morphing Wing UAVs," *Smart Materials and Structures*, Vol. 16, No. 3, June 2007, pp. 919–926.
doi:10.1088/0964-1726/16/3/042

[6] Xu, W., and King, T., "Flexure Hinges for Piezoelectric Displacement Amplifiers: Flexibility, Accuracy, and Stress Considerations," *Precision Engineering*, Vol. 19, No. 1, July 1996, pp. 4–10.
doi:10.1016/0141-6359(95)00056-9

[7] Moskalik, A. J., and Brei, D., "Quasi-Static Behavior of Individual C-Block Piezoelectric Actuators," *Journal of Intelligent Material Systems and Structures*, Vol. 8, No. 7, 1997, pp. 571–587.
doi:10.1177/1045389X9700800702

[8] Dogan, A., Uchino, K., and Newnham, R. E., "Composite Piezoelectric Transducer with Truncated Conical Endcaps Cymbal," *IEEE Transactions on Ultrasonics, Ferroelectrics, and Frequency Control*, Vol. 44, No. 3, May 1997, pp. 597–605.

doi:10.1109/58.658312
[9] Ervin, J. D., and Brei, D., "Recurve Piezoelectric-Strain-Amplifying Actuator Architecture," *IEEE/ASME Transactions on Mechatronics*, Vol. 3, 1998, pp. 293–301.
doi:10.1109/3516.736163
[10] Prechtl, E. F., and Hall, S. R., "Design of a High Efficiency, Large Stroke, Electromechanical Actuator," *Smart Materials and Structures*, Vol. 8, No. 1, 1999, pp. 13–30.
doi:10.1088/0964-1726/8/1/002
[11] Lee, T., and Chopra, I., "Design of Piezostack-Driven Trailing-Edge Flap Actuator for Helicopter Rotors," *Smart Materials and Structures*, Vol. 10, No. 1, 2001, pp. 15–24.
doi:10.1088/0964-1726/10/1/302
[12] Schwartz, R. W., and Narayanan, M., "Electroactive Apparatus and Methods," International Patent No. PCT/US02/09698, Clemson Univ., Clemson, SC, 28 March 2002.
[13] Mtawa, A., Sun, B., and Gryzagoridis, J., "An Investigation of the Influence of Substrate Geometry and Material Properties on the Performance of the C-Shape Piezoelectric Actuator," *Smart Materials and Structures*, Vol. 16, No. 4, 2007, pp. 1036–1042.
doi:10.1088/0964-1726/16/4/011
[14] Jiang, J., and Mockensturm, E., "A Motion Amplifier Using an Axially Driven Buckling Beam 1: Design and Experiments," *Nonlinear Dynamics*, Vol. 43, 2006, pp. 391–409.
doi:10.1007/s11071-006-0762-x
[15] Kim, J.-S.,Wang, K. W., and Smith, E. C., "Synthesis and Control of Piezoelectric Resonant Actuation Systems with Buckling-Beam Motion Amplifier," *AIAA Journal*, Vol. 46, No. 3, March 2008, pp. 787–791.
doi:10.2514/1.32216
[16] Kim, J.-S., Wang, K. W., and Smith, E. C., "Development of a Resonant Trailing-Edge Flap Actuation System for Helicopter Rotor Vibration Control," *Smart Materials and Structures*, Vol. 16, No. 6, Oct. 2007, pp. 2275–2285.
doi:10.1088/0964-1726/16/6/030
[17] Lesieutre, G., and Davis, C., "Transfer Having a Coupling Coefficient Higher than its Active Material," U.S. Patent 6,236,143, May 2001.
[18] Lesieutre, G., and Davis, C., "Can a Coupling Coefficient of a Piezoelectric Device Be Higher than Those of its Active Material?" *Journal of Intelligent Material Systems and Structures*, , Vol. 8, No. 10, 1997, pp. 859–867.
doi:10.1177/1045389X9700801005
[19] Barrett, R., and Tiso, P., "PBP Adaptive Actuator Device and Embodiments," International Patent Number: PCT/NL2005/000054 by Delft Univ. of Technology, 18 Feb. 2005.
[20] Clingman, D. J., and Ruggeri, R. T., "Mechanical Strain Energy Shuttle for Aircraft Morphing via Wing Twist or Structural Deformation," *Proceedings of SPIE: The International Society for Optical Engineering*, Vol. 5388, 2004, pp. 288–296.
doi:10.1117/12.538681
[21] Clingman, D. J., "Development of an Aerodynamic Synthetic Jet Actuator Based on a Piezoceramic Buckled Beam," M.S. Thesis, Univ. of Maryland, College Park, MD, Dec. 2006.
[22] DeBreuker, R., Tiso, P., Vos, R., and Barrett, R., "Nonlinear Semi-Analytical Modeling of Post- Buckled Precompressed (PBP) Piezoelectric Actuators for UAV Flight Control," 47th AIAA/ASME/ASCE/AHS/ASC Structures, Structural Dynamics and Materials Conference, AIAA Paper 2006-1795, Newport, RI, 1–4 May 2006.
[23] Giannopoulos, G., Monreal1, J., and Vantomme, J., "Snap-Through Buckling Behavior of Piezoelectric Bimorph Beams 1: Analytical And Numerical Modeling," *Smart Materials and Structures*, Vol. 16, No. 4, 2007, pp. 1148–1157.
doi:10.1088/0964-1726/16/4/024
[24] Barrett, R., McMurtry, R., Vos, R., DeBreuker, R., and Tiso, P., "Post-Buckled Precompressed Piezo-Electric Flight Control Actuator Design Development and Demonstration," *Smart Materials and Structures*, Vol. 15, No. 5, Oct. 2006, pp. 1323–1331.
doi:10.1088/0964-1726/15/5/022
[25] Vos, R., DeBreuker, R., Barrett, R., and Tiso, P., "Morphing Wing Flight Control via Post-Buckled Precompressed Piezoelectric Actuators," *Journal of Aircraft*, Vol. 44, No. 4, July–Aug. 2007, pp. 1060–1069.
doi:10.2514/1.21292
[26] Barrett, R., Vos, R., and DeBreuker, R., "Post-Buckled Precompressed (PBP) Subsonic Micro Flight Control Actuators and Surfaces," *Proceedings of SPIE: The International Society for Optical Engineering*, Vol. 6525, March 2007, Paper 65259M.
doi:10.1117/12.711561

C. Cesnik
Associate Editor